Journal of Network Intelligence
Taiwan Ubiquitous Information
 ISSN 2414-8105 (Online)
Volume **8**, Number **3**, August **2023**

Multi-objective Optimization Design and Dynamic Characteristic Analysis based on Planetary Gear Transmission

Qingyong Zhang[1], Saiyun Xu[1], Yiqing Yuan[1], Xiaolei Yan[1], Dengfeng Huang[1], Jie Yu[1]

[1] Shool of Mechanical and Automotive Engineering,
Fujian University of Technology, Fuzhou 350118, China
{24486416, 3367823553, 45740880, 345700653, 30498476, 95677615}@qq.com

Li Lin[2], Yong Wu[2], Guixian Zhan[2]

[2] Fujian Wanrun New Energy Technology Co., LTD, Fuzhou, China
{47355377, 413948347, 1172615096}@qq.com

Trong-The Nguyen[3,4]

[3] University of Information Technology, Ho Chi Minh City 700000, Vietnam
[4] Vietnam National University, Ho Chi Minh City 700000, Vietnam
thent@uit.edu.vn

*Corresponding authors: Qingyong Zhang

Received December 12, 2022, revised February 10, 2023, accepted April 3, 2023.

Abstract. *The planetary gear transmission of an electric bus is one of the most considered factors in bus design because it can reduce transmission noise and vibration during the design phase. This study investigates the gear micro-geometric optimization, and dynamic characteristic analysis of the transmission carried out while taking into account the meshing situation of the gear pair under various operating conditions. Gear micro modification parameters are optimized by multi-objective using the polynomial response surface agent model and Non-dominated Sorting in Genetic Algorithm-II (NSGA-II). The best gear modification parameters are obtained that then used with a Combination of Ordered Weighted Averaging (C-OWA) and Technique for Order Preference by Similarity to an Ideal Solution (TOPSIS) to perform the transmission planetary gear train's load tooth contact analysis (LTCA). A test bench is constructed for vibration testing, and the modal superposition method is employed to examine the investigated scheme's dynamic response of the transmission. The acoustic response of the transmission is then solved using the acoustic boundary element approach. The results demonstrate a significant reduction in the vibration and noise of the optimized transmission. The test results for vibration response align with those from the simulation, showing that the investigated scheme is safe and sound.*
Keywords: Planetary gear transmission; Vibration and noise; Modification parameters; Multi-objective optimization; Dynamic characteristic

1. **Introduction.** The Noise-Vibration-Harshness (NVH) is crucial for enhancing the comfort of a vehicle's ride [1]. The dynamic meshing force of the gear tooth is produced during transmission due to the elastic deformation of the gear under load, profile form distortion, and base pitch deviation [2]. Internal excitation, such as stiffness excitation, error excitation, and meshing impact excitation, impact the gear pair and cause gear vibration [3]. This vibration enters the box through the transmission shaft and bearing and

generates radiation noise. According to research, the load-bearing gear pair's transmission error during the meshing process is the primary source of excitation for transmission vibration noise [4]. When the transmission error is consistent, the gear won't vibrate [5, 6]. Gear micro-modification can reduce transmission vibration noise and tooth surface load deviation, increase gear life, and enhance transmission error fluctuation [7].

The polynomial response surface surrogate model of gear modification parameters and maximum contact stress proposed in 2015 based on the Monte Carlo method [8]. The amount of gear modification through an optimization algorithm [9] developed based on improved gears' contact condition and transmission stability but at the expense of a high computational load [10]. Similarly, it reached the ideal amount of gear modification, proposed based on enhancing the dynamic performance of the gear system, but box deformation into account neglected to take [11]. Using the genetic algorithm for improving the transmission's noise issue under the second gear's 40% working condition without taking contact under other working situations into account [12]. Micro-modification optimization of gear has attracted wide attention from scholars [13] with a dual-objective function optimization model of gear transmission error and tooth surface contact stress by combining tooth profile and tooth direction modification to obtain the optimal modification amount of helical gear through a genetic algorithm [14, 15], which minimized the noise of the reducer but did not take into account other load conditions [16]. An optimized the transmission error fluctuation of gear pairs, considered the tooth profile and longitudinal modification parameters as the design variables [17, 18], and exploited the response surface method to obtain the optimal modification parameters of helical planetary gear train gears [19]. Improvement in the vibration and noise of the gear system, but the authors did not consider the influence of other modification parameters. Recent literature ignores the differences between gear pairs under various operating situations and the deformation of flexible parts, instead simply taking into account a particular load condition or observing the response of the gear transmission system.

The objective of this paper is to use an electric bus to lessen the vibration and noise of a planetary gear transmission. The micro-modification of the gear is optimized using a multi-objective genetic algorithm, and the dynamic and auditory responses of the transmission under various load circumstances are studied. Finally, the veracity of the analysis is confirmed by the transmission test bench.

2. **Modeling Analysis and Influence Parameters.** The related work consists of the subsections of modeling analysis and influence parameters.

2.1. **Modeling Analysis.** The analysis includes construction, simulation analysis, and boundary load ratio. Construction is a as rigid-flexible coupling simulation analysis model of the transmission is proposed, as shown in Figure 1, taking into account the planetary gear transmission, the input revolution speed fluctuation, bearing stiffness, gear meshing characteristics, connection relationship of gear components, and the flexible characteristics of the transmission shell [2].

With solar wheels as input and planet carrier as output, the main parameters of the planetary gear train are shown in Table. 1.

According to the actual use of the transmission, set the corresponding load conditions, as shown in Table. 2.

Simulation analysis is as considering the strength and life of the gear system, vibration, and noise, the rigid-flexible coupling model of transmission is analyzed, as shown in Table. 3.

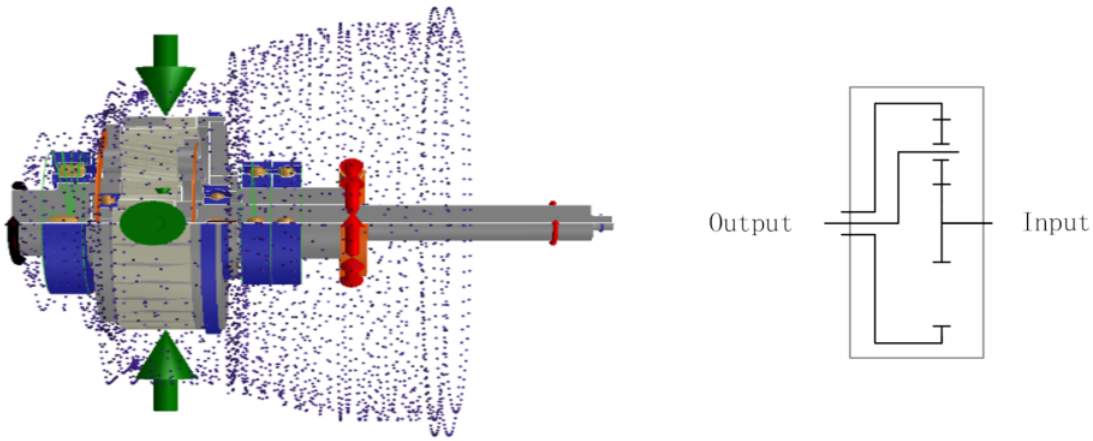

FIGURE 1. A rigid-flexible coupling model

TABLE 1. The main parameters of the electric bus planetary gear

Name/Parameter	Sun gear	Planetary gear	Ring gear
Number of teeth z	37	23	83
Tooth width b/mm	40	38.5	52
Normal modulus m_n/mm	2.28		
Pressure angle α/deg	20		
Helix Angle β/deg	14		

TABLE 2. A load cases of gearbox in the electric bus planetary gear

Load cases	Duration(hrs)	Temperature(C)	Input speed(rpm)	Input torque(Nm)
100%Load	600	70	2000	1000
75%Load	600	70	2000	750
50%Load	600	70	2000	500
25%Load	600	70	2000	250

The following notations are defined in Table 3, $K_{H\beta}$ is the contact tooth surface load coefficient; ΔTE is the transmission error fluctutation; F is the max contact stress; q is the max Load per unit length; η is the boundary load ratio(defined as the ratio of the peak load at the tooth face boundary to the peak load on the entire tooth face) [20]; SH is the gear contact safety factor; SF is the gear bending safety factor; left tooth surface of planetary gear stands of the working tooth surface of the planetary gear when the sun gear is engaged with the planetary gear; the right tooth surface of the planetary gear stands of the working tooth surface of the planet gear when the ring gear is engaged with the planet gear [2, 3].

Boundary Load Ratio: in the process of gear meshing, the uneven Load will cause the abnormal operation of the gear, resulting in pitting, cracks and other problems of the gear, and at the same time aggravate the gear noise. In severe cases, there will be broken teeth. The boundary load ratio describes the ratio of the peak load at the tooth surface boundary to the peak load on the entire tooth surface during gear transmission. The smaller the boundary load ratio is, the less obvious the gear eccentric load is when the boundary load ratio is equal to 0, the gear will not have eccentric load [21]. Therefore,

TABLE 3. Relevant data of working tooth surface of 100% Load planetary gear

Related parameter	Left tooth surface of planetary	Right tooth surface of planetary	Reference value
$K_{H\beta}$	2.85	1.11	≤1.45
ΔTE/um	2.39	0.76	≤1
F/MPa	1391	761	≤1500
q/N/mm	248	97.8	≤300
η	1	1	≤0.5
SH	0.89	1.32	≥1.05
SF	1.46	1.51	≥1.2

the uneven Load of the gear can be effectively improved by reducing the boundary load ratio.

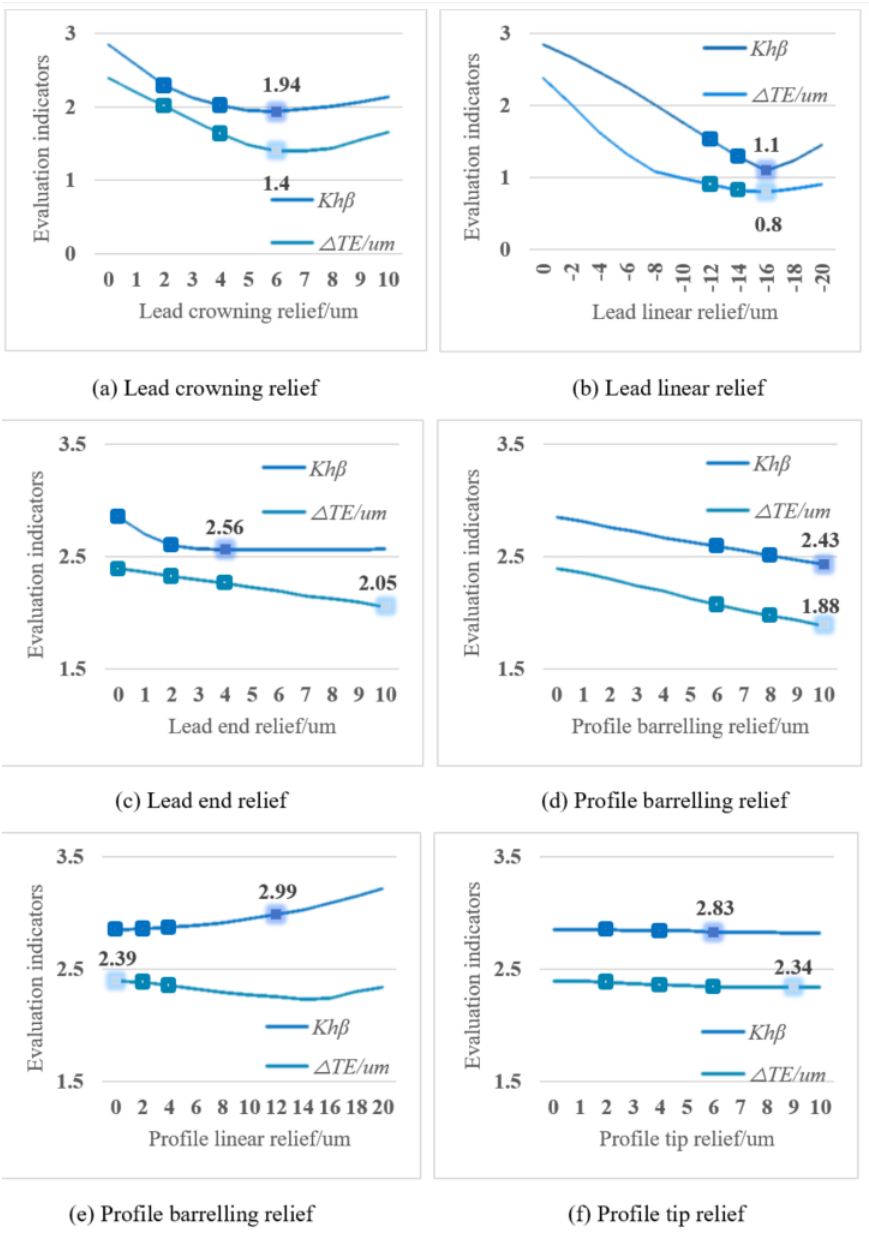

FIGURE 2. Curves of transmission error fluctuation and contact tooth load coefficient with gear modification

Taking the left tooth surface of planetary gear as an example, the influence of gear modification parameters such as lead crowning relief, lead linear relief, profile barreling relief and profile linear relief on transmission error fluctuation and contact tooth surface load coefficient is analyzed, and the minimum point of both data annotations is shown in Figure 2.

3. **Multi-Objective Optimization.** This section suggested a novel scheme of gear micro-geometric optimization for electric bus planetary gear transmission using a multi-objective function for gear micro modification parameters based on the polynomial response surface agent model and Non-dominated Sorting in Genetic Algorithm-II (NSGA-II)[22]. We also carried out the dynamic characteristic analysis of the transmission while considering the gear pair's meshing situation under various operating conditions. The results are presented in the conclusion of the analysis and discussion.

3.1. **Problem Optimization Model.** Taking the modification parameters of the left tooth surface of the planetary gear as the design variables, the minimum of the transmission error fluctuation, the boundary load ratio and the contact tooth surface load coefficient as the optimization objective, a multi-objective optimization model is established as follows:

$$\min \begin{cases} y_1(x_1, x_2, x_3, x_4, x_5, x_6) \\ y_2(x_1, x_2, x_3, x_4, x_5, x_6) \\ y_3(x_1, x_2, x_3, x_4, x_5, x_6) \end{cases} \tag{1}$$

s.t.

$$\{2 \le x_1 \le 6,\ -16 \le x_2 \le -12,\ 0 \le x_3 \le 4, 6 \le x_4 \le 10, 0 \le x_5 \le 4, 2 \le x_6 \le\ 6,\ y_1 \le 1$$
$$y_2 \le 0.5,\ y_3 \le 1.45,\ x_1, x_2, x_3, x_4, x_5, x_6 \in 0.1N\ \}$$

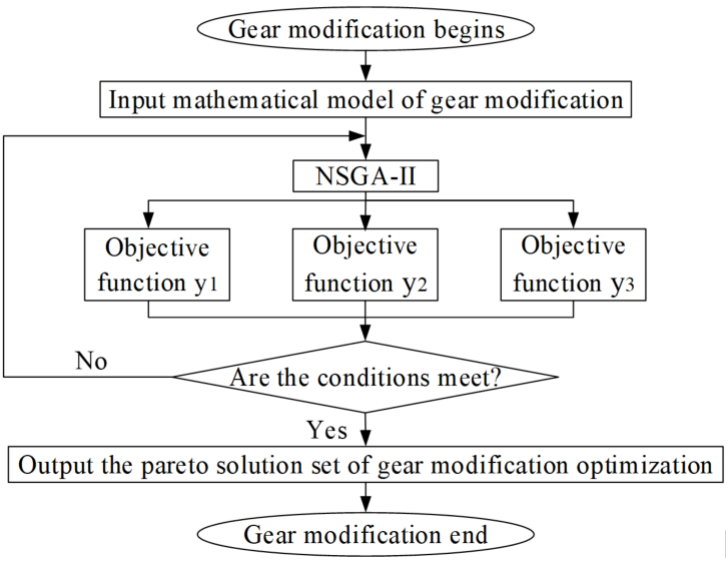

FIGURE 3. A optimal flow chart of gear modification

Optimization method: Non-dominated Sorting in Genetic Algorithm-II (NSGA-II) [22] is a multi-objective genetic algorithm. NSGA-II considers the partially ordered set, focusing distance and elitist strategy, and has the characteristics of low time complexity

and good solution set convergence. Thus, it can effectively solve nonlinear optimization problems. The process of gear modification optimization is shown in the flowchart in Figure. 3. Optimization setting: The initial population number of NSGA-II is set to

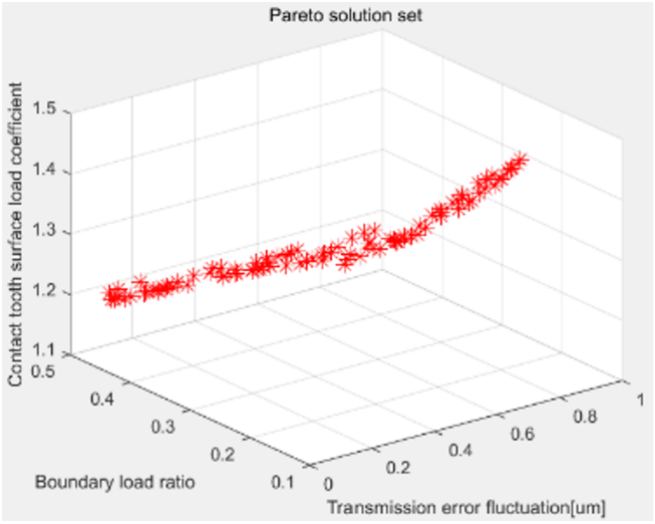

FIGURE 4. An example of a real closed house used in actual mapping construction

100, and the maximum number of iterations to 500 [25]. The crossover probability is 0.8, and the mutation probability is 0.05. The Pareto solution set obtained by MATLAB programming [26], as shown in Figure 4.

3.2. **Polynomial Response Surface Surrogate Model.** The polynomial response surface surrogate model [24] is a mathematical model that fits the relationship between input and output, and its expression is given as follows.

$$y_k = c_0 + \sum_{i=1}^{n} c_i x_i + \sum_{i=1}^{n} \sum_{j=i}^{n} c_{ij} x_i x_j \tag{2}$$

$$(k = 1, 2, \ldots, m; i = 1, 2, \ldots, n; j = i, \ldots, n),$$

where, y_k is defined as the objective function, k is the k_{th} objective function, When $m = 3, y_1, y_2, y_3$ correspond to the transmission error fluctuation, the boundary load ratio and the contact tooth surface load coefficient, respectively; c_0, c_i, c_{ij} represent the undetermined coefficients [17], respectively; x_i, x_j are the design variable; and the number of design variables are denoted by n, When $n = 6, x_1, x_2, \ldots, x_6$ correspond to lead crowning relief, lead linear relief, lead end relief, profile barreling relief, profile linear relief and profile tip relief, respectively [18]. Coefficient of determination(R^2)indicates the fitting degree of the model. As the accuracy of the surrogate model improves, the value of R^2 approaches to 1, and is mathematically represented by.

$$R^2 = 1 - \frac{S_E}{S_T} = \frac{S_R}{S_T} \tag{3}$$

where S_T is the sum of the squares of the total deviation; S_R is the regression sum of squares; and S_E represents the sum of squared residuals. According to the analysis of gear modification parameters based on specific number 2.1 pitch, the forward search method is used to draw up the range of parameter values and obtain the orthogonal factor level. When the radial crown is $6um$, the transmission error fluctuation and the contact

TABLE 4. Factor with levels sets of um

Factor/Level	x_1	x_2	x_3	x_4	x_5	x_6
-1	2	-16	0	6	0	2
0	4	-14	2	8	2	4
1	6	-12	4	10	4	6

TABLE 5. Response surface test design and results

Serial number	$x_1, x_2, x_3, x_4, x_5, x_6$	y_1	y_2	y_3
1	2,-16,2,10,2,4	0.45	0.43	1.21
2	6,-12,2,10,2,4	1.15	0.28	1.61
3	4,-14,4,10,2,6	0.85	0.22	1.44
4	2,-14,2,10,0,4	0.45	0.57	1.23
…	…	…	…	…
51	4,-14,4,6,2,6	0.64	0.43	1.48
52	6,-14,4,8,2,2	1.02	0.43	1.64
53	4,-12,0,8,4,4	0.72	0.50	1.43
54	4,-16,2,8,4,6	0.71	0.36	1.43

load coefficient of the left tooth surface of the planetary gear reaches a minimum, so the orthogonal test levels of the radial crown are 2, 4 and 6um [2].

On the other hand, the fluctuation of the transmission error of the left tooth surface in the planetary gear reaches a minimum when the modification amount of the parabola at both ends is 4um, while the load coefficient of the contact tooth surface reaches a minimum when the modification amount of the parabola at both ends is 10um. Therefore, the orthogonal test levels of the crown amount in the tooth direction are 0, 2 and 4um. Similarly, the orthogonal test levels of other modification parameters can be obtained, for which the results are shown in Table. 4.

where x_1, x_2, x_3, x_4, x_5 and x_6 represent lead crowning relief, lead linear relief, lead end relief, profile barreling relief, profile linear relief and profile tip relief, respectively. Considering the stability of gear transmission, the partial Load and uneven distribution of tooth surface load, Load Tooth Contact Analysis for the sample point of Table 4 is carried out. The transmission error fluctuation, boundary load ratio and contact tooth surface load coefficient of the left tooth surface of planetary gear under different modification parameters are obtained, as shown in Table 5.

In Table 5, x_1, x_2, x_3, x_4, x_5, and x_6 are defined as gear profile modification parameter; y_1 represents the transmission error fluctuation; y_2, the boundary load ratio; and y_3, the contact tooth surface load coefficient. From the above analysis of the response surface model of lead relief, profile relief and other modification parameters, the transmission error fluctuation can be obtained as follows.

$$y_1 = -0.64812+0.23208x_1 -0.016771x_2+0.12146x_3+0.020208x_4+0.0096875x_5+0.025417x_6 - 0.0053125x_1x_2 -0.017813x_1x_3 -0.00515625x_1x_4 -0.00875x_1x_5 -0.010313x_1x_6+0.0021875x_2x_3 -0.00 34375x_2x_4+0.00265625x_2x_5+0.000625x_2x_6 -0.0028125x_3x_4 -0.0015625x_3x_5+0.005625x_3x_6+0.0075 x_4x_5+0.0009375x_4x_6 -0.000625x_5x_6+1.74097E\text{-}017x_1^2 -0.0021875x_2^2+1.07 11E\text{-}017x_3^2 -0.000625x_4^2+0.00125x_5^2+0.0021875x_6^2.$$

Similarly, the boundary load ratio can be obtained as.

TABLE 6. The Pareto optimal initial data

Expert/Aim	y_1	y_2	y_3	Expert/Aim	y_1	y_2	y_3
A	8	8	8	F	9	8	6
B	9	8	6	G	10	9	8
C	8	8	6	H	8	9	8
D	8	8	9	I	10	8	6
E	10	9	9	J	10	9	8

y_2 =4.27833−0.42361x_1+0.28785x_2 −0.15722x_3 −0.12701x_4+0.00652778x_5 −0.058924x_6 −0.013125 x_1x_2 +0.026875 x_1x_3 − 0.011406 x_1x_4 +0.0084375 x_1x_5 +0.000625 x_1x_6 − 0.008125 x_2x_3 +8.58644E-017x_2x_4 −0.0021875x_2x_5+9.50642E018x_2x_6 −0.015312x_3x_4 −0.00375x_3x_5 −0.0032812 5x_3x_6 −0.0090625x_4x_5+0.0021875x_4x_6 −0.004375x_5x_6+0.027014x_1^2+0.00690972x_2^2+0.00899306x_3^2+ 0.011701x_4^2+0.00722222x_5^2+0.00586806x_6^2.

Finally, the contact tooth surface load coefficient is expressed as follows.

y_3 =1.43542+0.060972x_1+0.073681x_2+0.029861x_3+0.052569x_4+0.014444x_5+0.011493x_6 −0.0040625 x_1x_2 −0.0078125x_1x_3 −0.00140625x_1x_4+0.001875x_1x_5 −0.0059375x_1x_6 −0.00062x_2x_3 −0 0003125 x_2x_4 −2.60209E-018x_2x_5+2.14661E-018x_2x_6 −0.000625x_3x_4 −3.83323E−020 x_3x_5+0.00296875x_3x_6 −0.00125x_4x_5+4.29322E-018x_4x_6+1.53329E-018x_5x_6+0.00253472x_1^2+ 0.00159722x_2^2+0.000659722x_3^2 −0.00340278x_4^2 −0.00246528x_5^2+0.00128472x_6^2.

3.2.1. *C-OWA calculation with the target weight.*

1. The initial data $(a_1, a_2, \ldots, a_n)$ is obtained by inviting n experts to evaluate the importance of m objectives (transmission error fluctuation, boundary load ratio and contact tooth surface load coefficient). This is followed by arranging the initial data in descending order to obtain the updated data $(b_1, b_2, \ldots, b_n)$[3].
2. Apply combination $C^j_{(n-1)}$, to calculate a weighted vector is as ω follows.

$$\omega = C^j_{n-1} / \sum_{j=0}^{n-1} C^j_{n-1} = C^j_{n-1}/2^{n-1}, (j = [0, n-1], n = 10) \tag{4}$$

3. Obtain an absolute weight with weighted and updated data $\overline{\omega_i}$ follows.

$$\overline{\omega_i} = \sum_{j=0}^{n-1} w \cdot b_j \, (i = [1, m], m = 3; j = [0, n-1], n = 10) \tag{5}$$

4. convert the absolute weight to obtain a relative weight ω_i.

$$\omega_i = \overline{\omega_i} / \sum_{i=1}^{m} \overline{\omega_i} \;\; (i = [1, m], m = 3) \tag{6}$$

The initial data is shown in Table. 6, resulting in the calculated weight vector, $\omega(0.002, 0.018,\ 0.07, 0.164, 0.246, 0.246, 0.164, 0.070, 0.018, 0.002)$, the absolute weights, $\overline{\omega_i}(9.162, 8.868, 7.146)$ and the relative weights, $\omega_i(0.364, 0.352, 0.284)$. In the Table 6. A domination of A to J that symbol of the expert/aim series.

3.2.2. *TOPSIS method calculation.* TOPSIS is used for the target comprehensive evaluation index, which are steps as follows.

1. Write the set of Pareto optimal solutions in the form of the matrix Y[3].

$$Y = (y_{ij})_{m \times n} \quad , (i = [1, m], \ m = 100; \ j = [1, n], n = 3), \tag{7}$$

TABLE 7. According to the actual situation of contact chart, the top 10 selected solutions in Pareto optimal solution set

N	$x_1, x_2, x_3, x_4, x_5, x_6$	y_1, y_2, y_3	C_i^*
1	2,-16,3.4,9.3,0.7,2.5	0.41,0.35,1.25	0.563255
2	2.3,-16,3.6,8.4,1.4,3.9	0.47,0.29,1.31	0.553602
3	2,-16,4,9.4,1.5,2.9	0.46,0.31,1.27	0.547977
4	2,-16,3,9.4,0,2.4	0.38,0.4,1.23	0.546078
5	2.3,-16,4,8.4,1.5,3.9	0.49,0.28,1.33	0.540947
6	2.1,-16,4,9.4,1.5,2.9	0.48,0.3,1.28	0.535852
7	2,-16,4,9.4,1.5,3.5	0.49,0.29,1.29	0.533932
8	2.6,-16,4,8.7,1.5,3.1	0.52,0.27,1.33	0.519552
9	2.6,-16,3.6,8.4,1.4,3.9	0.52,0.27,1.34	0.519228
10	2.1,-164,9.4,1.5,3.9,	0.52,0.28,1.3	0.512226

where m is the number of Pareto optimal solutions for gear modification parameters; and n represents the number of objectives corresponding to each group of solutions.

2. Normalize the matrix Y to obtain the canonical matrix Z.

$$Z = (z_{ij})_{m\times n} = \left(y_{ij} / \sqrt{\sum_{i=1}^{m} y_{ij}^2} \right)_{m\times n} \tag{8}$$

$(i = [1, m], m = 100; j = [1, n], n = 3)$.

3. Each element of the canonical matrix Z is weighted to obtain a weighted canonical matrix X.

$$X = (x_{ij})_{m\times n} = \omega_j \cdot z_{ij} \ , \tag{9}$$

with setting as following, $(i = [1, m], m = 100; j = [1, n], n = 3)$.

4. The minimum element of each column in the normalized weight matrix X is taken as an ideal solution x_j^*, and the maximum elements are taken as a negative ideal solutions x_j^0.

$$x_j^* = min_{x_{ij}}, \ x_j^0 = max_{x_{ij}} \ \ (i = [1, 100] \, ; \ j = [1, 3]) \, , \tag{10}$$

with setting as following, $(i = [1, m], m = 100; j = [1, n], n = 3)$.

5. Calculate the distance d_i^* from the ideal solution of each element of the weighted gauge matrix X and the distance d_i^0 from the negative ideal solution.

$$d_i^* = \sqrt{\sum_{j=1}^{n} \left(x_{ij-x_j^*}\right)^2} \ , \ d_i^0 = \sqrt{\sum_{j=1}^{n} \left(x_{ij-x_j^0}\right)^2} \ , \tag{11}$$

with setting as following, $(i = [1, 100]; j = [1, n], n = 3)$.

6. The comprehensive evaluation index C_i^* of each scheme is calculated and sorted in descending order to find the best scheme.

$$C_i^* = d_i^0 / \left(d_i^0 + d_i^*\right) , \ (i = [1, 100]) \, , \tag{12}$$

In combination with the actual situation of contact spots, the top 10 sequences of comprehensive evaluation are selected as shown in Table 7. The content values in Table 7, N is the sequence number and C_i^* is the comprehensive evaluation index. The design variable corresponding to the highest value of the comprehensive evaluation index in Table 7 is selected as the left tooth surface modification parameter of the planetary gear. Table 8 shows the right tooth surface modification parameter of the planetary gear is obtained after appropriate adjustment, in which N is the sequence number, d_1 and d_2 represents

TABLE 8. Modification parameters of working tooth surface of planet gear

N	Parameter	Planetary gear left tooth surface	Planetary gear right tooth surface
1	x_1 (um)	2	2
2	x_2 (um)	-16	0
3	x_3 (um)	3.4	3.4
4	d_1 (mm)	0.684	0.684
5	x_4 (um)	9.3	9.3
6	x_5 (um)	0.7	0.7
7	x_6 (um)	2.5	2.5
8	d_2 (mm)	1.368	1.368

the end relief length and tip relief length, respectively. It can be seen that the suggested

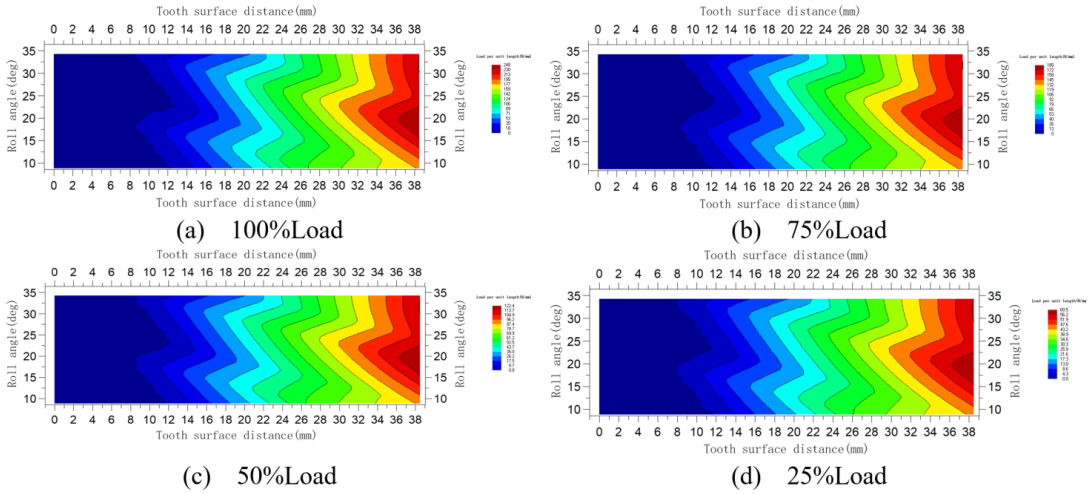

FIGURE 5. Contact chart on the left tooth surface of the planetary wheel under different loading conditions before modification

scheme performs smoothly the left tooth surface of the planetary wheel under different loading conditions before modification.

3.3. **Comparison of results.** The working tooth surface of the planetary gear is optimized by using the above modification parameters. Figures 5 to 8 show the contact spot diagram of the gear pair before and after modification.

Therefore, the eccentric Load of the planetary gear is improved, reducing the peak load of the tooth root and the tooth top. Improvement is also observed in the meshing quality of the gear pair and a reduction in the gear's impact and the gear's vibration. Finally, the gear transmission performance and service life is improved.

Utilizing the simulation data from Table 3, further analysis of the planetary gear working tooth parameters is performed under different load conditions [27]. Specifically, contact tooth surface load coefficient, transmission error fluctuation, maximum contact stress, maximum unit length load, boundary load ratio, gear contact safety factor and gear bending safety factor of the working tooth surface of the planetary gear are analyzed under different load conditions. The obtained results are shown in Tables 9 and 10. In the Tables, they can be seen that the suggested scheme offers the better in comparison of the gear before and after modification in both left and right of the tooth surface.

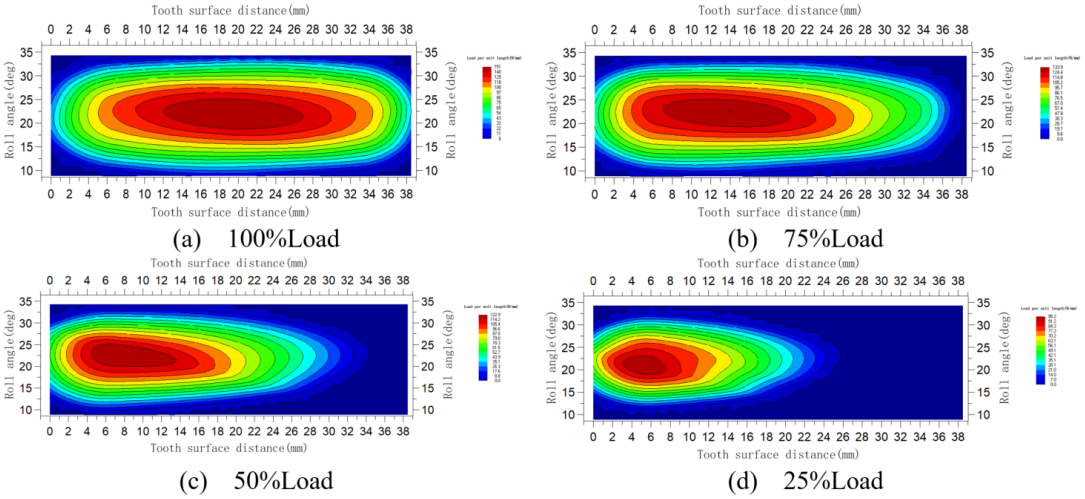

FIGURE 6. Contact chart on the left tooth surface of the planetary wheel under different loading conditions after modification

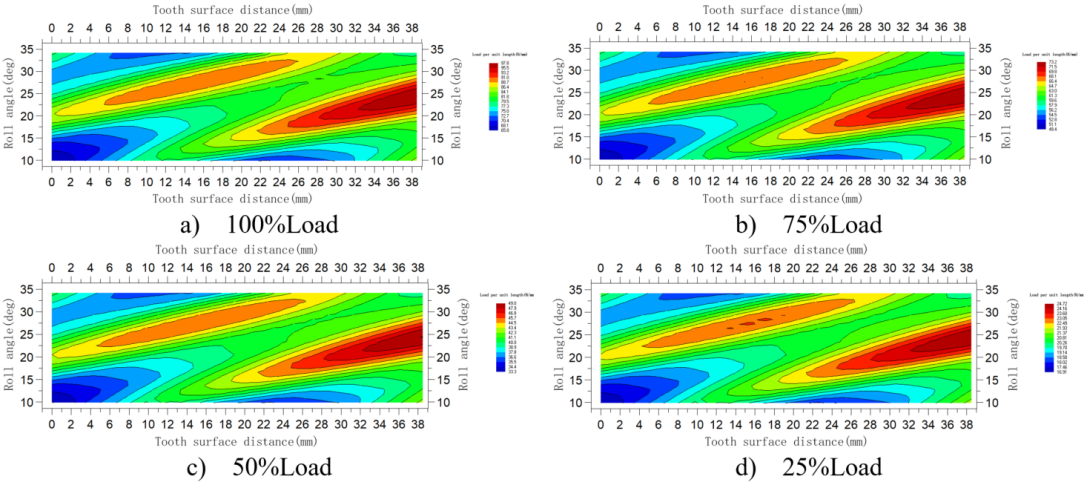

FIGURE 7. Contact chart on the right tooth surface of the planetary wheel under different loading conditions before modification

TABLE 9. The planet wheel works (left) on the tooth surface

condition index	100%Load		75%Load		50%Load		25%Load	
	Before	After	Before	After	Before	After	Before	After
$K_{H\beta}$	2.85	1.23	2.84	1.36	2.81	1.70	2.81	1.70
ΔTE	2.39	0.43	1.79	0.58	1.19	0.77	1.19	0.77
F	1391	973	1202	915	981	872	981	872
q	248	151	185	133.9	122.4	123.1	122.4	123.1
η	1	0.36	1	0.43	1	0.50	1	0.50
SH	0.89	1.1626	0.99196	1.2863	1.1444	1.4377	1.1444	1.4377
SF	1.46	2.2651	1.813	2.7667	2.4203	3.4825	2.4203	3.4825

A good trend is observed after the optimization of the working condition index of the meshing gear pair of the planetary gear train, fulfills which fulfills the requirement of different working conditions. In particular, most of the models used in this transmission are medium and heavy load conditions, so the load coefficient of the contact tooth surface

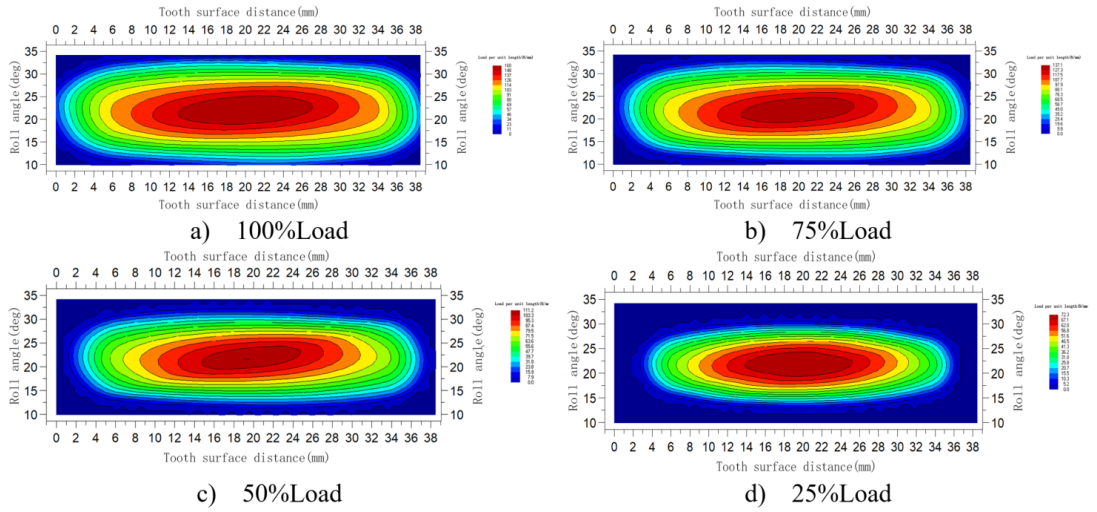

FIGURE 8. Contact chart on the right tooth surface of the planetary wheel under different loading conditions before modification

TABLE 10. The planet wheel works (right) on the tooth surface

Working Condition index	100%Load		75%Load		50%Load		25%Load	
	Before	After	Before	After	Before	After	Before	After
$K_{H\beta}$	1.11	1.27	1.11	1.34	1.11	1.45	1.11	1.55
ΔTE	0.76	0.52	0.58	0.62	0.40	0.65	0.21	0.20
F	761	682	659	625	540	556	386	451
q	97.6	160	73.2	137.1	49	111.2	24.97	72.3
η	1	0.29	1	0.14	1	0.07	1	0
SH	1.3224	1.4158	1.4368	1.5271	1.6051	1.684	1.9095	1.9902
SF	1.5065	1.6797	1.7806	1.9576	2.227	2.3929	3.1778	3.3681

slightly exceeds the reference value under low load condition, which can be ignored due of its negligible impact.

4. **Analysis and Discussion Results.** Through observed results of gear stiffness excitation, error excitation and meshing impact excitation, we used the kinetic response [28] with being calculated as following equation.

$$[M]\left\{\ddot{x}\right\} + [C]\{\dot{x}\} + [K]\{x\} = \{F(t)\} \tag{13}$$

where $[M]$, $[C]$, and $[K]$ are the mass matrix, damping matrix and stiffness matrix, respectively, while $\{\ddot{x}\}, \{\dot{x}\}, \{x\}$, and $F(t)$ represents the acceleration, velocity, displacement, and excitation vector, respectively [21].Considering the gear stiffness excitation, error excitation and meshing impact excitation, the internal excitation of the gear can be expressed as follows.

$$F(t) = \Delta k(t) \cdot \mathrm{e}(t) + S(t) \ , \tag{14}$$

where $F(t)$ is the internal incentives; $\Delta k(t)$ represent the variable of meshing stiffness; $e(t)$ and $S(t)$ are the gear composite error (including tooth profile error and base pitch error) and meshing impact excitation, respectively. In this paper, the influence of gear error [29] on internal excitation is considered, and the modal superposition method [29] is used to solve the acceleration, velocity and displacement response of the shell, which is

represented as follows.

$$x = \psi\eta = \sum_{i=1}^{m} \Phi_i \eta_i \tag{15}$$

where x is the displacement vector corresponding to each node degree of freedom; ψ is the vibration mode matrix; η is the modal coordinate vector; Φ_i is the i_{th} order modal vibration vector; and η_i represents the first modal coordinate [30]. Figure 9 shows the vibration acceleration response results of the simulation measuring points on the shell surface in the X, Y and Z directions. It can be seen from the above analysis that the

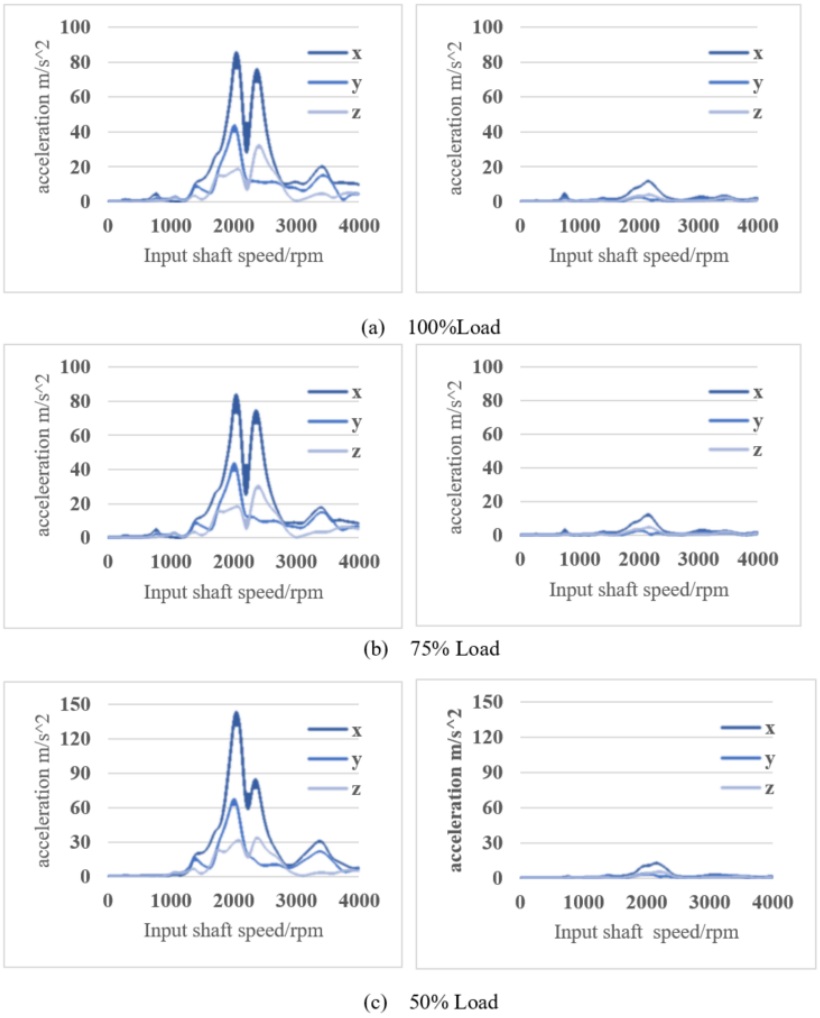

FIGURE 9. Vibration acceleration response at node 25040 of casing surface before and after modification

acceleration response amplitude in X direct-ion is most obvious when the gear tooth engagement order is 25.592 and the corresponding acceleration response peak values of 100% 25% Load before and after modification are $90m/s^2, 85m/s^2, 140m/s^2, 70m/s^2$ and $12m/s^2, 12m/s^2, 12m/s^2, 16m/s^2$ [30].

4.1. **Test Verification Results.** In order to further verify the validity of the simulation results, a transmission vibration test bench is built, which mainly includes three parts: input, load motor bench and transmission assembly [31]. Figure 10 displays a transmission vibration test bench device and Transmission vibration test bench device diagram. It

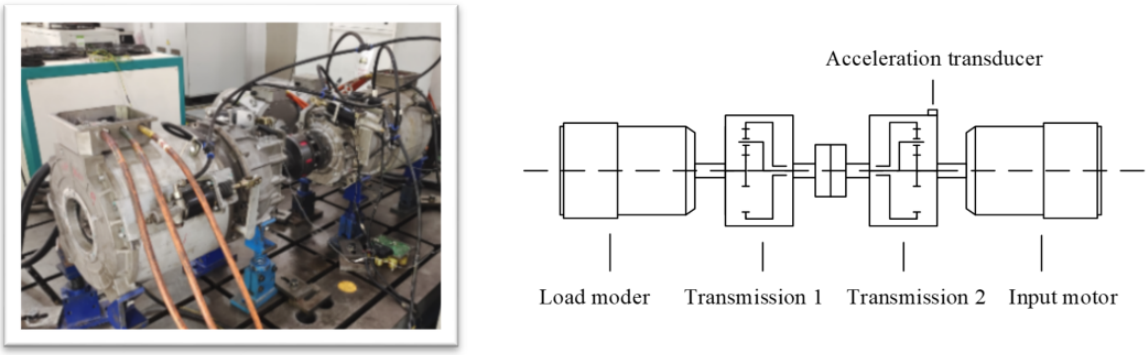

a) Transmission vibration test bench device b) Transmission vibration test bench device diagram

FIGURE 10. Transmission vibration test bench device and transmission vibration test bench device diagram

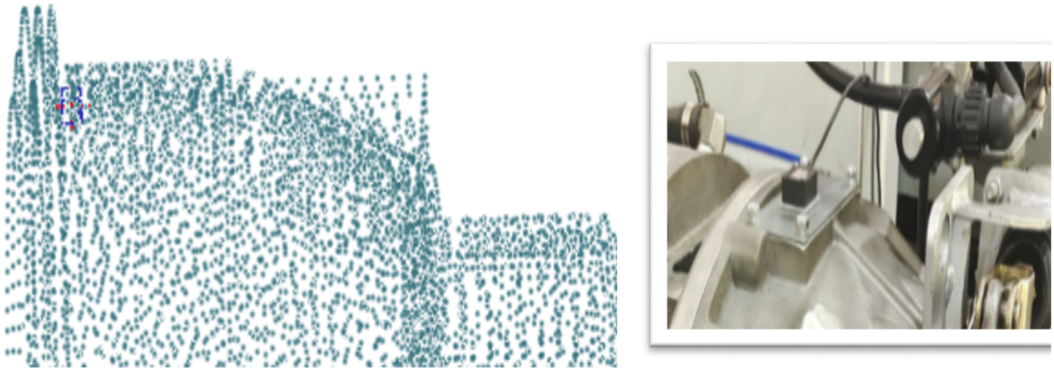

a) Simulation measuring point b) Test poin

FIGURE 11. Transmission vibration test bench device with measuring and testing points

is The load motor control speed, input motor control torque, transmission test bench diagram.

Figure 11 shows a three component accelerator in used to log the vibration response of the transmission. It is an installation position of acceleration sensor with a set the test torque to $250Nm$ and vary the speed from 100 to $3800rpm$.

Figure 12 shows a transmission vibration bench test process and the vibration acceleration test results. Thus, the vibration test results of the gearbox under the acceleration condition are obtained, and the corresponding order is obtained 25.592. The acceleration test results of the shell surface test point in the X direction. It was observed that for the optimized transmission, the acceleration response results of the simulation measuring points on the shell surface are consistent with the test measuring points, which shows the viability of the simulation results.

4.2. **Radiated Noise Analysis.** Theoretical analysis, it is a system equation for calculating the sound pressure on the surface of the structure using the direct boundary element method is given as follows.

$$A(\omega)\, p = B(\omega)\, v_n \tag{16}$$

where A, B are the influence matrices; p is the surface nodal pressure; and v_n, the normal velocity of surface nodes. At any point p_r in the sound field r, the sound pressure can be

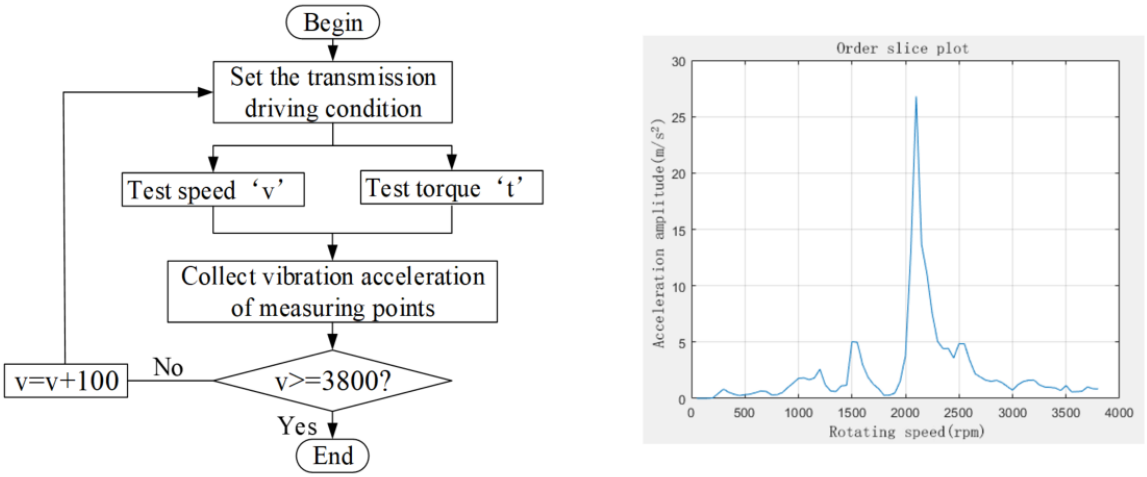

a) Transmission vibration bench test process b)Vibration acceleration test results

FIGURE 12. Transmission vibration bench test process and the vibration acceleration test results

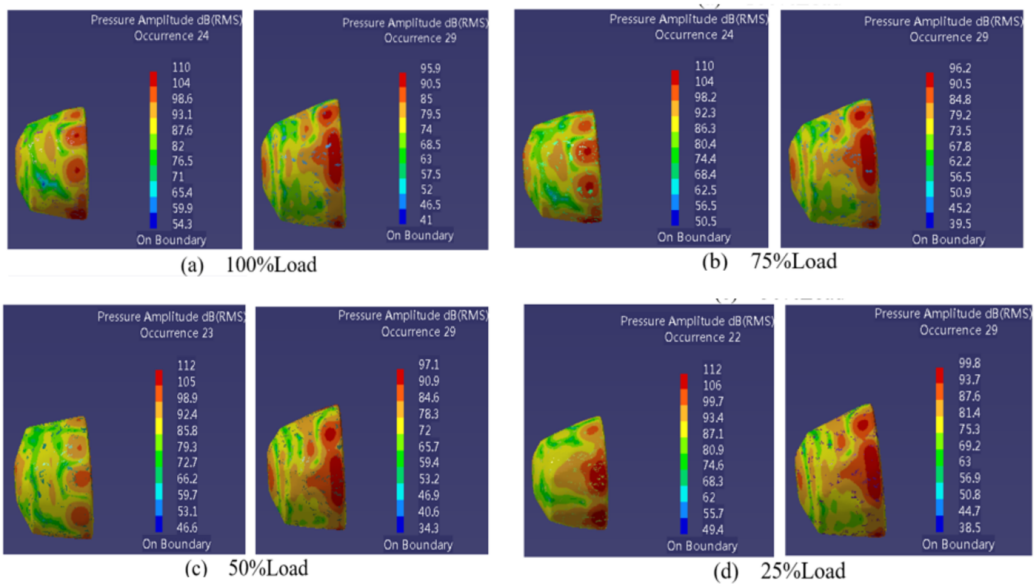

(a) 100%Load (b) 75%Load

(c) 50%Load (d) 25%Load

FIGURE 13. Housing surface sound pressure under different loading conditions before and after modification

calculated as.

$$p_r = C^T p + D^T v_n \tag{17}$$

where C and D are the coefficient matrices.

Simulation analysis: Further comparative analysis of the acoustic response of the transmission before and after optimization. Established the boundary element model of the transmission, and set the reference sound pressure to $2 \times^{-5} Pa$, the reference sound intensity to $1 \times^{-12} w/m^2$, the air density to $1.225 kg/m^3$, the speed of sound is $340 m/s$. Perform Fourier transform on the speed response results of the box to obtain the corresponding frequency response, which is used as the boundary condition of the acoustic response to calculate the acoustic measurement of the box surface under different load conditions. Figure 13 shows a housing surface sound pressure under different loading conditions before and after modification. It is seen that the surface sound pressure values of the shell

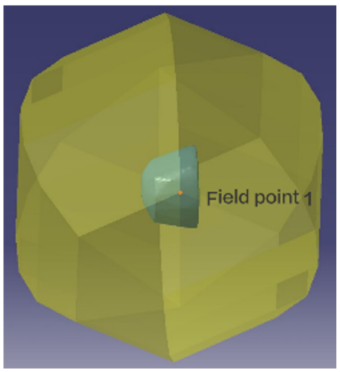

FIGURE 14. A spherical sound field

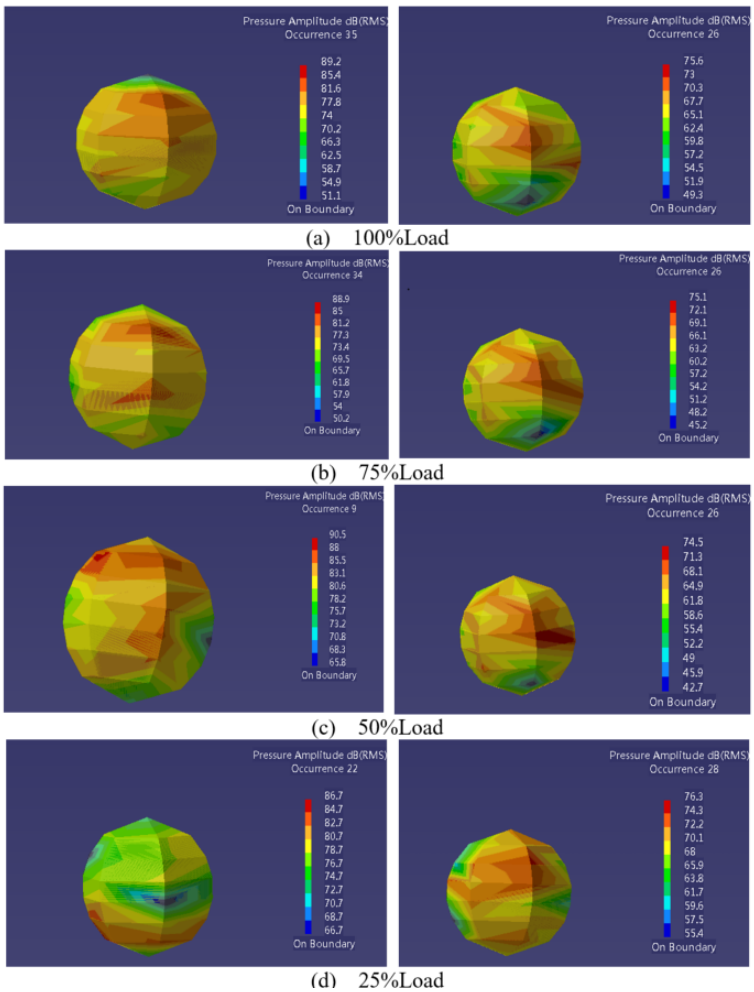

FIGURE 15. A field point sound pressure level cloud image under different loading conditions before and after modification

before the modification are $110dB, 110dB, 112dB$ and $112dB$, respectively, and the surface sound pressure values of the shell after modification are $95.9dB, 96.2dB$, $97.1dB$ and $99.8dB$, respectively. A spherical sound field of the transmission with a radius of 1m as shown in Figure 14 is established, and the sound pressure response of the sound field is calculated. Figure 15 shows a peak sound pressure level response of the sound field before and after modification under different load conditions.

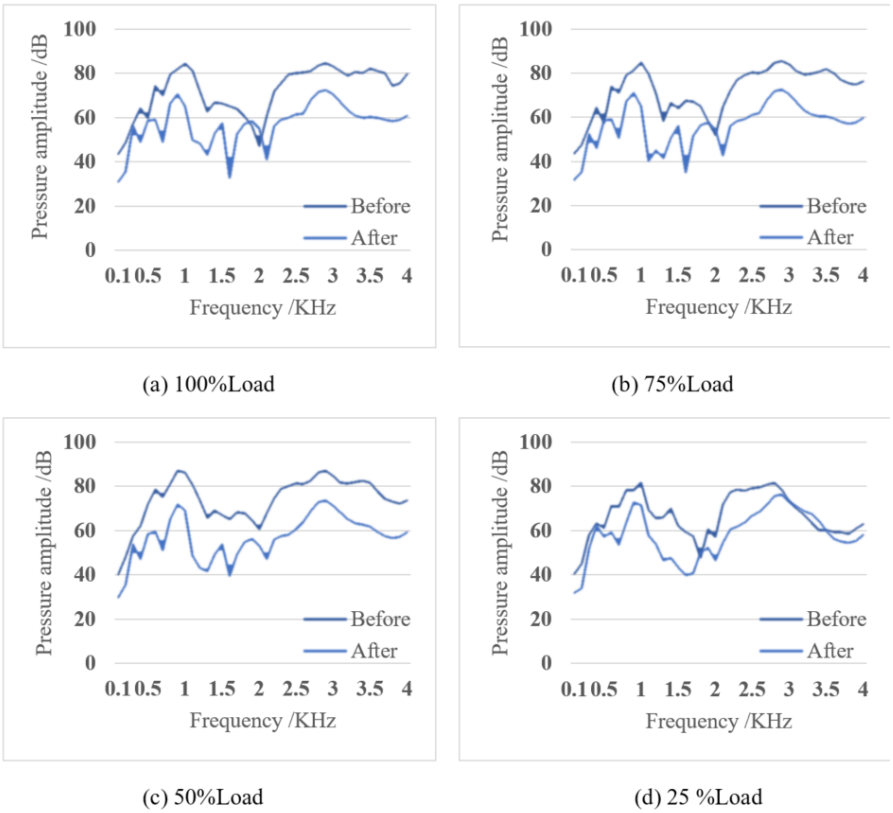

FIGURE 16. Sound pressure level distribution curve of field point 1 under different load condition

Considering the sequence of load conditions in Figure 15(a)∼(d), the peak sound pressure levels of the sound field before the modification are $89.2dB, 88.9dB, 90.5dB$ and $86.7dB$, respectively, and the peak sound pressure levels of the good field after conversion are $75.6dB, 75.1dB, 74.5dB$, and $76.3dB$, respectively. Figure 16 displays the radiation noise of field point 1 under different load conditions is calculated, and the sound pressure level distribution curve. Examining the sequence of load conditions in Figure 16(a)∼(d), the maximum sound pressure levels of the gearbox before modification are $84.71dB, 85.65dB, 87.26dB$ and $81.71dB$, respectively.
The maximum sound pressure levels of the gearbox after modification are $72.46dB, 72.7dB, 73.62dB$ and $76.35dB$. Thus, a reduction of $12.25dB, 12.95dB, 13.64dB$, and $5.36dB$ is observed which results in the reduction of noise in the gearbox and fulfills the use of multiple working conditions.

5. **Conclusions.** This study suggested a novel scheme of gear micro-geometric optimization for electric bus planetary gear transmission. We introduced a multi-objective function for gear micro modification parameters based on the polynomial response surface agent model and Non-dominated Sorting in Genetic Algorithm-II (NSGA-II). The dynamic characteristic analysis of the transmission are carried out while considering the gear pair's meshing situation under various operating conditions. Some achieved results are concluded as follows. (1) The rigid-flexible coupling model of the planetary gear transmission is created, and the response of the model under various load situations is investigated, taking into account the deformation of the flexible system components; (2) A boundary load ratio idea is proposed, and the smallest boundary load ratio is considered as one of the optimization objectives, enhancing the load contact between the

tooth root and tooth top in the direction of tooth width and tooth profile; (3) A forward search approach is suggested to identify the range of modification parameters, such as tooth drum shape and tooth tilt, taking the accuracy of the polynomial response surface surrogate model into consideration; (4) Considering the strength and life, vibration and noise of the gear system, the polynomial response surface surrogate model of transmission error fluctuation, boundary load ratio, contact surface load coefficient, and modification parameters was established, and the optimal modification parameters were determined by combining NSGA-II, C-OWA operator and TOPSIS method; (5) Examining the use of the transmission under different working conditions, the dynamic response and acoustic response of the transmission under other working conditions are analyzed, and the effectiveness and accuracy of the optimization results are verified by the vibration bench test, which validates the vibration and noise reduction of the transmission and has practical engineering significance.

Acknowledgments. This project is supported by the project of scientific research foundation of Fujian University of Technology (GY-Z20170) and the Fujian Provincial Department of Finance (GY-Z21004).

REFERENCES

[1] D. Mundo, "Geometric design of a planetary gear train with non-circular gears", *Mechanism and Machine Theory*, vol. 41, no. 4, pp. 456–472, 2006.

[2] H. Abderazek, S. M. Sait, and A. R. Yildiz, "Optimal design of planetary gear train for automotive transmissions using advanced meta-heuristics, *International Journal of Vehicle Design*, vol. 80, no. 2–4, pp. 121–136, 2019.

[3] T. L. Hill, Statistical mechanics: principles and selected applications, *Courier Corporation*, 2013.

[4] C. R. Patil, P. P. Kulkarni, N. N. Sarode, and K. U. Shinde, "Gearbox noise & vibration prediction and control," *International Research Journal of Engineering and Technology*, vol. 4, pp. 873–877, 2017.

[5] Z. Yuan, Z. L. Sun, and D. Wang, "GA-based optimum profile modification of spur gears for vibration damping," *Journal of Northeastern University (Natural Science)* , vol. 31, no. 6, pp. 873–876, 2010.

[6] T.-T. Nguyen, J.-S. Pan, T.-Y. Wu, T.-K. Dao, and T.-D. Nguyen, "Node Coverage Optimization Strategy Based on Ions Motion Optimization," *Journal of Network Intelligence*, vol. 4, no. 1, pp. 1–9, 2019.

[7] C. Wang, "Optimization of tooth profile modification based on dynamic characteristics of helical gear pair," *Iranian Journal of Science and Technology, Transactions of Mechanical Engineering*, vol. 43, no. 1, pp. 631–639, 2019.

[8] S.-J. Kim, C.-H. Kim, S.-Y. Jung, and Y.-J. Kim, "Optimal design of novel pole piece for power density improvement of magnetic gear using polynomial regression analysis," *IEEE Transactions on Energy Conversion*, vol. 30, no. 3, pp. 1171–1179, 2015.

[9] L. Kang, R.-S. Chen, Y.-C. Chen, C.-C. Wang, X. Li, and T.-Y. Wu, "Using Cache Optimization Method to Reduce Network Traffic in Communication Systems Based on Cloud Computing," *IEEE Access*, vol. 7, pp. 124397–124409, 2019, doi: 10.1109/ACCESS.2019.2938044.

[10] T.-T. Nguyen, J.-S. Pan, S.-C. Chu, J. F. Roddick, and T.-K. Dao, "Optimization Localization in Wireless Sensor Network Based on Multi-Objective Firefly Algorithm," *Journal of Network Intelligence,* vol. 1, no. 4, pp. 130–138, 2016.

[11] G.-Z. Fu, H.-Z. Huang, Y.-F. Li, B. Zheng, and T. Jin, "Multi-objective design optimization for a two-stage transmission system under heavy load condition," *Mechanism and Machine Theory,* vol. 122, pp. 308–325, 2018.

[12] F. Mendi, T. Başkal, K. Boran, and F. E. Boran, "Optimization of module, shaft diameter and rolling bearing for spur gear through genetic algorithm," *Expert Systems with Applications,* vol. 37, no. 12, pp. 8058–8064, 2010.

[13] T.-Y. Wu, J. C. Lin, Y. Zhang, and C.-H. Chen, "A Grid-Based Swarm Intelligence Algorithm for Privacy-Preserving Data Mining," *Applied Sciences,* vol. 9, no. 4, 774, 2019, doi: 10.3390/app9040774.

[14] L. Kang, R. Chen, N. Xiong, Y. Chen, Y. Hu, and C. Chen, "Selecting Hyper-Parameters of Gaussian Process Regression Based on Non-Inertial Particle Swarm Optimization in Internet of Things," *IEEE Access,* vol. 7, pp. 59504–59513, 2019.

[15] F. Zhang, T.-Y. Wu, Y. Wang, R. Xiong, G. Ding, P. Mei, and L. Liu, "Application of Quantum Genetic Optimization of LVQ Neural Network in Smart City Traffic Network Prediction," *IEEE Access,* vol. 8, pp. 104555–104564, 2020.

[16] B. Akay, D. Karaboga, B. Gorkemli, and E. Kaya, "A survey on the artificial bee colony algorithm variants for binary, integer and mixed integer programming problems," *Applied Soft Computing,* vol. 106, p. 107351, 2021.

[17] S. Kumar, A. Damaraju, A. Kumar, S. Kumari, and C. M. Chen, "LSTM Network for Transportation Mode Detection," *Journal of Internet Technology,* vol.22, no. 4, pp.891-902, 2021.

[18] E. K. Wang, F. Wang, S. Kumari, J. H. Yeh, and C. M. Chen, "Intelligent monitor for typhoon in IoT system of smart city," *The Journal of Supercomputing*, vol. 77, no. 3, pp. 3024-3043, 2021.

[19] Y. Lei, L. Hou, Y. Fu, J. Hu, and W. Chen, "Research on vibration and noise reduction of electric bus gearbox based on multi-objective optimization," *Applied Acoustics*, vol. 158, p. 107037, 2020.

[20] T.-T. Nguyen, T.-D. Nguyen, and V.-T. Nguyen, "An Optimizing Pulse Coupled Neural Network based on Golden Eagle Optimizer for Automatic Image Segmentation," *Journal of Information Hiding and Multimedia Signal Processing,* vol. 13, no. 3, pp. 155–164, 2022.

[21] T. K. Dao, T. S. Pan, T. T. Nguyen, and S. C. Chu, "A compact Articial bee colony optimization for topology control scheme in wireless sensor networks," *Journal of Information Hiding and Multimedia Signal Processing,* vol. 6, no. 2, pp. 297–310, 2015.

[22] K. Deb, S. Agrawal, A. Pratap, and T. Meyarivan, "A fast elitist non-dominated sorting genetic algorithm for multi-objective optimization: NSGA-II," *Parallel Problem Solving from Nature PPSN VI,* pp. 849–858, 2000.

[23] Y. Li and Y. Chen, "Genetic ant algorithm for continuous function optimization and its MATLAB implementation," *in Proceedings - 2010 International Conference on Intelligent System Design and Engineering Application, ISDEA 2010*, 2011, vol. 1, pp. 791–794.

[24] P. Gao, H. Liu, P. Yan, Y. Xie, C. Xiang, and C. Wang, "Research on application of dynamic optimization modification for an involute spur gear in a fixed-shaft gear transmission system," *Mechanical Systems and Signal Processing*, vol. 181, p. 109530, 2022.

[25] T.-Y. Wu, L. Wang, X. Guo, Y.-C. Chen, and S.-C. Chu, "SAKAP: SGX-Based Authentication Key Agreement Protocol in IoT-Enabled Cloud Computing," *Sustainability,* vol. 14, no. 17, 11054, 2022, doi: 10.3390/su141711054.

[26] T.-Y. Wu, Q. Meng, S. Kumari, and P. Zhang, "Rotating behind Security: A Lightweight Authentication Protocol Based on IoT-Enabled Cloud Computing Environments," *Sensors,* vol. 22, no. 10, 3858, 2022, doi: 10.3390/s22103858.

[27] J. A. Korta and D. Mundo, "Multi-objective micro-geometry optimization of gear tooth supported by response surface methodology," *Mechanism and Machine Theory,* vol. 109, pp. 278–295, 2017.

[28] T. Lin, H. Cao, and H. Lyu, "Vibration noise prediction and tooth modification effect analysis of a fourstage planetary gearbox," *Journal of Chongqing University*, vol. 44, no. 09, pp. 14–20, 2018.

[29] Z. Peng, J. Liu, F. Xiong, and et al., "Study on Gear Whine of Hybrid Power System based on Contact Patch and Micro Modification," *Journal of Mechanical Transmission*, vol. 16, no. 20, pp. 14–20, 2020.

[30] L. Zhao, M. Du, and Y. Yang, "Optimizing gear micro geometry for minimum transmission error when considering manufacturing deviation," *International Journal of Materials, Mechanics and Manufacturing,* vol. 6, no. 1, pp. 74–77, 2018.

[31] F. Zhan and J. Xu, "Virtual Lab Acoustics simulation computing from beginner to proficient," *Northwestern Polytechnical University*, p. 477, 2013.